Oxidation of Metals, Vol. 58, Nos. 3/4, October 2002 (© 2002)

Water Vapor and Oxygen/Sulfur-Impurity Effects on Oxidation and Nitridation in Single- and Two-Phase Cr–Nb Alloys

M. P. Brady,*† P. F. Tortorelli,* and L. R. Walker*

Received October 4, 2001; revised March 8, 2002

The oxidation and nitridation behavior of Cr(Nb) solid solution and Cr_2Nb Laves phase was studied individually and in combination at 1100°C and 950°C in dry air, humid air, and N_2–$4H_2$ for alloys containing high or low levels of oxygen and sulfur impurities. At 1100°C, humid-air exposure of alloys in which the Cr_2Nb phase was the matrix resulted in greatly increased subscale nitridation as compared with exposure in dry air. At 950°C, little difference between dry vs. humid-air exposures was observed; however, greatly increased subscale nitridation was observed in the Cr_2Nb-matrix eutectic alloy when the levels of oxygen and sulfur impurities in the alloys were reduced. In contrast, unalloyed Cr and Cr(Nb) solid-solution alloys were relatively insensitive to water vapor or impurity oxygen/sulfur effects under the conditions studied, although the addition of Nb as a solute in Cr did increase the extent of subscale nitridation. Possible synergistic effects between sulfur impurities and water vapor in the Cr_2Nb alloys and the possibility for similar effects in other intermetallic systems are discussed.

KEY WORDS: Cr; Cr_2Nb laves phase; sulfur; water vapor; oxidation; nitridation.

INTRODUCTION

Laves-phase strengthened Cr alloys are being developed for use at high temperatures in aggressive oxidation and hot-corrosion environments.[1–10] The

*Metals and Ceramics Division, Oak Ridge National Laboratory, Oak Ridge, Tennessee 37831-6115.
†To whom all correspondence should be sent; email: BradyMP@ornl.gov

0030-770X/02/1000-0000/0 © 2002 Plenum Publishing Corporation

Cr(X)–Cr_2X systems of interest (X = Hf, Nb, Ta, Zr) typically contain eutectic reactions. The Cr_2X particles provide high-temperature strength and the Cr(X) phase is a potential source of ductility and oxidation/corrosion resistance.

Binary alloys based on the Cr(Ta)–Cr_2Ta eutectic were recently shown to exhibit superior oxidation resistance to similar Cr(Nb)–Cr_2Nb alloys at 1100°C in humid air.[11] Further development of these alloys has resulted in oxidation resistance comparable to that of conventional, commercial Cr_2O_3-forming alloys.[10] Given the similarities between Nb and Ta, the superior oxidation resistance of the Cr(Ta)–Cr_2Ta alloys is considered surprising.

To gain an understanding of this effect, the oxidation behavior of the Cr(X) solid-solution phase and Cr_2X Laves phase (X = Nb, Ta) was investigated individually and in combination from 950–1100°C in dry and humid air. Of particular importance for Cr alloys is the formation of Cr_2N subscales in air, which can grow at a much higher rate than Cr_2O_3 and rapidly embrittle and consume a component.[12] This paper presents some unusual and surprising effects of exposures in dry air vs. humid laboratory air and low vs. high levels of alloy oxygen and sulfur impurities on subscale nitridation in the Cr(Nb)–Cr_2Nb system. Details of oxidation behavior in the Cr(Ta)–Cr_2Ta system and possible reasons for their superior oxidation resistance relative to Cr(Nb)-Cr_2Nb alloys are presented elsewhere.[13,14]

EXPERIMENTAL

Small 50–60 g castings of unalloyed Cr, Cr(Nb), Cr_2Nb, and Cr(Nb) + Cr_2Nb alloys were prepared by arc-melting and drop casting in a chilled-copper mold. The work focused on three alloys (all compositions reported in atomic percent, at.%): Cr–2.5Nb to represent the Cr(Nb) solid-solution phase (Cr–1Nb was also studied), Cr–31Nb to represent the Cr_2Nb Laves phase, and the two-phase Cr(Nb)–Cr_2Nb eutectic composition Cr–18.5Nb (Fig. 1 and Table I). The compositions of the single-phase Cr–2.5Nb and Cr–31Nb alloys were selected to extend slightly into the two-phase Cr(Nb) + Cr_2Nb field to allow comparison of behavior at equivalent Cr and Nb activities and are referred to as "single-phase" for convenience. The eutectic Cr–18.5Nb composition consisted of a Cr_2Nb matrix with Cr(Nb) second-phase particles.[2,15]

The commercial-purity (CP) Cr source used to make the alloys was found to contain high levels of oxygen and sulfur (Table I). Accordingly, selected alloys were recast with high-purity (HP) Cr supplied by JMC (Research Triangle Park, North Carolina) to provide a basis for comparison. This effect was further studied for the eutectic alloy Cr–18.5Nb by doping the HP Cr arc-melting charge with Cr_2O_3 (HP + oxygen) or Cr_2S_3

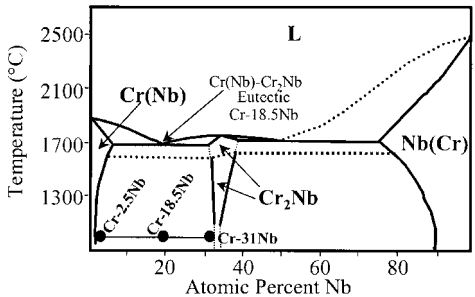

Fig. 1. Schematic binary Cr–Nb phase diagram. From Ref. 15.

Table I. Alloy Compositions Measured by Inductively Coupled Plasma Spectroscopy and Combustion Techniques

Alloy	Nb (at.%)	Impurities (weight ppm) O	N	C	S
CP–Cr	—[a]	7340	60	200	330
HP–Cr	—	158	24	<100	<10
UHP–Cr	—	20	<3	<100	<10
CP Cr–1Nb	0.78	6890	50	200	360
HP Cr–1Nb	1.03	158	24	<100	<10
CP Cr–2.5Nb	2.48	7225	47	<100	320
HP Cr–2.5Nb	2.50	82	<3	<100	<10
CP Cr–18.5Nb	18.19	4711	41	<100	220
HP Cr–18.5Nb	18.53	29	<3	<100	<10
HP Cr–18.5Nb + Cr_2O_3	17.92	4947	34	<100	30
HP Cr–18.5Nb + Cr_2S_3	18.02	172	2	<100	280
CP Cr–31Nb	30.69	3780	50	100	200

[a]—, not present.

(HP + sulfur) powder (Table I). Some ultrahigh-purity Cr (UHP) Cr, also provided by JMC, was remelted, and used for comparison with the oxidation behavior of unalloyed CP and HP Cr. To simplify sample description, *no label signifies an alloy made from CP Cr.*

Unless otherwise noted, the alloys were vacuum heat-treated at 1300°C for 24 hr and furnace cooled. Disk-shaped specimens of approximately 12–13-mm diameter and 1–1.5-mm thickness were polished to a 600-grit finish using SiC paper. Surface cracks were present in the Cr_2Nb Laves-phase alloy Cr–31Nb; further, the brittleness of this alloy necessitated the use of irregular shaped test coupons. Oxidation behavior was studied by thermogravimetric analysis (TGA) at 1100 and 950°C in filtered compressed dry

air or open to "laboratory" air of varying daily relative humidity (usually 50% range). Typically, duplicate TGA runs were performed for all alloy/condition/environment data presented. Selected samples were also placed in alumina crucibles (with lids) and isothermally or cyclically exposed (air cooled to room temperature after 1, 4, 10, 30, 48, and 120 cumulative hr) at 1100°C in a tube furnace open to humid laboratory air for periods up to a week. As expected for this temperature, there was some volatility, which was evident by green "stains" on the inside of the lids. However, volatility-related weight loss did not appear to be significant compared to weight gains under the conditions studied. Several samples were also nitrided for 24 hr at 1100°C in a vacuum furnace backfilled with N_2–$4H_2$ (the hydrogen was added to prevent oxidation and the cross sections were checked by SEM to ensure that no significant oxide-scale formation occurred). Oxidized and nitrided coupons were characterized by X-ray diffraction (XRD), light microscopy, secondary-mode scanning-electron microscopy (SEM), and electron-probe microanalysis (EPMA) using pure-element standards for Cr, Nb, Ta, a BN standard for N, and an Al_2O_3 standard for O.

RESULTS

Kinetics in Dry and Humid Air at 1100°C

For Cr–2.5Nb, Cr–18.5Nb, and Cr–31Nb, the rates of oxidation at 1100C in dry air were somewhat similar (Fig. 2a). The Cr_2Nb Laves-phase alloy (Cr–31Nb) exhibited the slowest oxidation rate of the three alloys and the Cr(Nb) alloy (Cr–2.5Nb) was the fastest. The two-phase Cr(Nb) + Cr_2Nb eutectic alloy Cr–18.5Nb exhibited oxidation kinetics intermediate between that of Cr–2.5Nb and Cr–31Nb. In humid air (Fig. 2b), Cr–2.5Nb showed similar oxidation kinetics to that observed in dry air (Fig. 2a). However, the oxidation rates of Cr–18.5Nb and Cr–31Nb were markedly greater in humid air. The Cr–31Nb alloy showed a transition to rapid linear-oxidation kinetics after ~10 hr at 1100°C. The Cr–18.5Nb alloy exhibited similar rapid linear kinetics, but, unlike Cr–31Nb, it did not show much of an initial parabolic region; consequently, its overall weight gain after 24 hr was higher than that of Cr–31Nb (Fig. 2b). Therefore, the combination of the Cr(Nb) and Cr_2Nb phases in a eutectic mixture resulted in faster oxidation kinetics in humid air than either single-phase Cr(Nb) or Cr_2Nb.

Some sample-to-sample variation in oxidation rate was encountered in the TGA data for the Cr–2.5Nb samples run in both dry and humid air for 24 hr at 1100°C. Additional 24-hr TGA runs were conducted for Cr–2.5Nb in dry and humid air using as-cast and heat-treated coupons made from CP

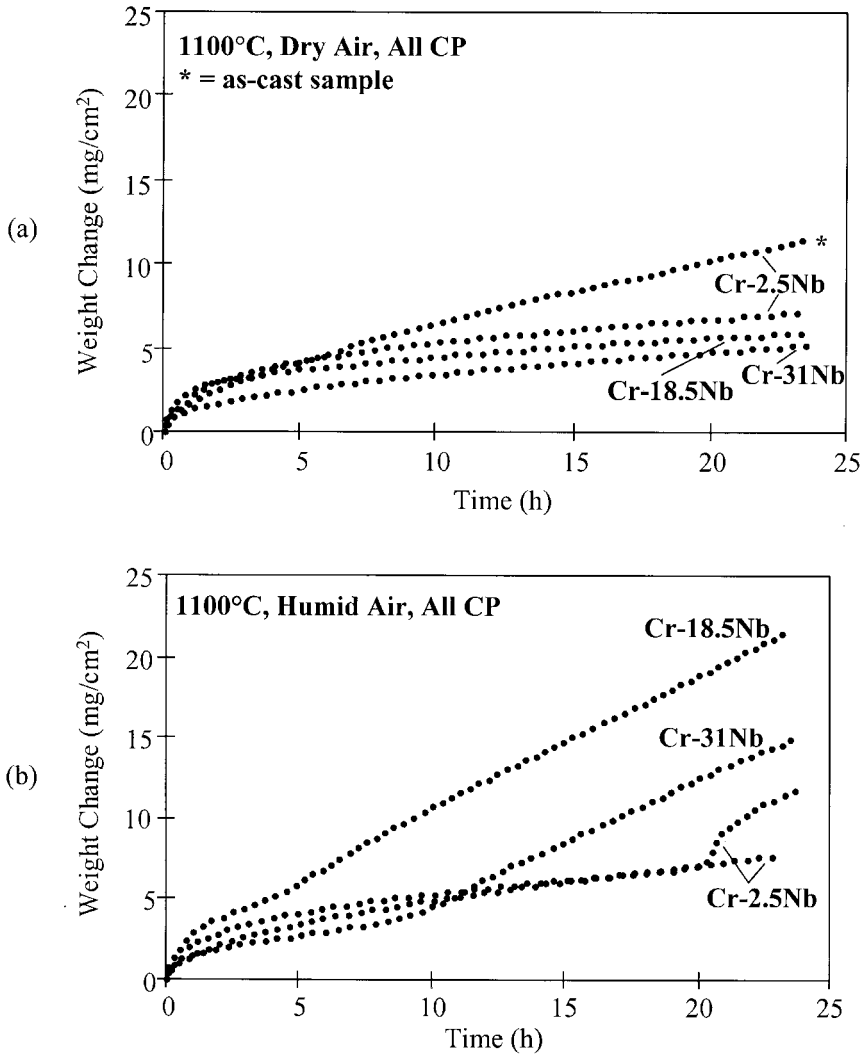

Fig. 2. TGA data at 1100°C for commercial-purity (CP) Cr–2.5Nb (single phase), Cr–18.5Nb (two-phase Cr–Cr_2Nb eutectic), and Cr–31Nb (single-phase Cr_2Nb Laves phase) alloys exposed in filtered compressed dry air (a) and in humid laboratory air (b).

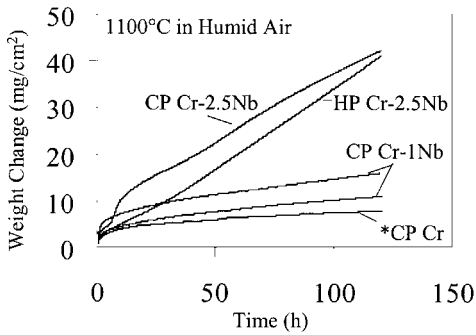

Fig. 3. TGA data for CP and HP Cr–2.5Nb, CP Cr–1Nb, and CP Cr alloys exposed for 120 hr at 1100°C in humid laboratory air.

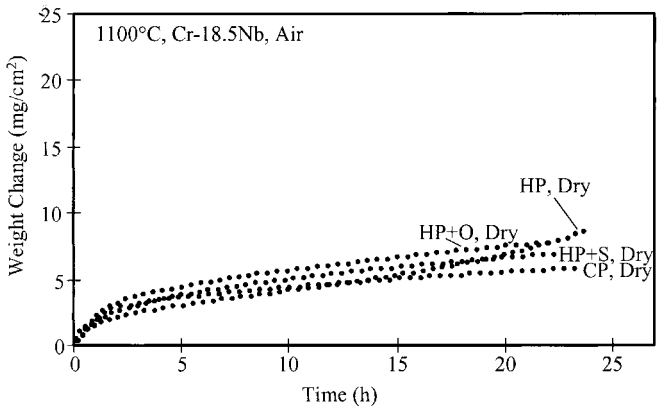

Fig. 4. TGA data at 1100°C in filtered compressed dry air for CP, HP, HP + oxygen, and HP + sulfur Cr–18.5Nb.

or HP Cr. No consistent pattern emerged among these factors. Longer-term, 120-hr exposures were conducted at 1100°C in humid air for CP and HP Cr–2.5Nb, as well as CP Cr–1Nb and unalloyed CP Cr (Fig. 3). These data indicated that Cr–2.5Nb (CP and HP) exhibits a transition to rapid linear-oxidation kinetics in the one 24-hr time range at 1100°C in humid air (Figs. 2b and 3). The unalloyed Cr and Cr–1Nb exhibited more parabolic-like kinetics and much lower weight gains over the course of the 120-hr exposure.

Figure 4 shows TGA data at 1100°C in dry air for Cr–18.5Nb with different levels of impurities (CP, HP, HP + oxygen, HP + sulfur). All of the

alloys exhibited similar, relatively low rates of oxidation in dry air, although the TGA curve for the HP alloy did show an increased oxidation rate after about 15 hr of exposure. A HP Cr–18.5Nb alloy sample was also oxidized at 1100°C in humid air for a 1-cycle, 24-hr exposure and a 6-cycle, 120-hr cumulative exposure, both of which showed the large weight gains similar to that observed for CP Cr–18.5Nb exposed in humid air (Fig. 2b).

Oxidized Microstructures for 1100°C Exposures

The Cr_2O_3 scales formed on nearly all the Cr–Nb alloys studied (CP and HP, dry and humid air) were locally convoluted and, thus, highly friable. Such local friability led to bands of disconnected Cr_2O_3 particles on top of the scale during metallographic preparation, such as is evident in Fig. 5a for a Cr–2.5Nb exposed for 24-hr at 1100°C in humid air. In some samples/sample regions, this layer spalled during cooling or metallographic handling and is, therefore, not evident in all the cross sections.

Cr(Nb) Phase: Cr–2.5Nb

At 1100C, a Cr_2O_3 scale in the 25-μm range (not including the outer friable zone) was formed on Cr–2.5Nb samples exposed for 24 hr in both dry and humid air. For most samples, extensive spallation occurred during air cooling to room temperature. The sample-to-sample variation in TGA data was found to be reflected in the cross-section microstructures. The lower rates of oxidation corresponded to the presence of a dense, continuous Cr_2O_3 scale with no evidence of underlying subscale reaction (Fig. 5a, which also shows a remaining fragment of the porous, loosely adherent outer scale). In contrast, the samples that showed the higher rates of oxidation exhibited nitridation to form a subscale of average composition 61Cr–1Nb–38N (Fig. 5b). XRD of similarly exposed samples indicated that this phase was Cr_2N. The depth of the nitride subscale after 24 hr of exposure varied greatly from sample to sample, with the greatest depth of nitridation, 80 μm, observed for the as-cast sample exposed in dry air (cf. TGA data in Fig. 2a).

The samples showing nitride subscales also exhibited a qualitative tendency for the overall Cr_2O_3 scale to be more porous (compare Fig. 5a and b, noting that much of the Cr_2O_3 had spalled in the sample shown in 5b). Because of scale spallation, it is not clear if the porous Cr_2O_3 was the initial scale formed on the alloy. If so, the formation of a nitride subscale could have occurred because the scale would not have been an effective reaction barrier. However, it is also possible (and more likely) that this Cr_2O_3 was formed upon subsequent oxidation of the Cr_2N subscale and, thus, was a consequence of the subscale nitridation.

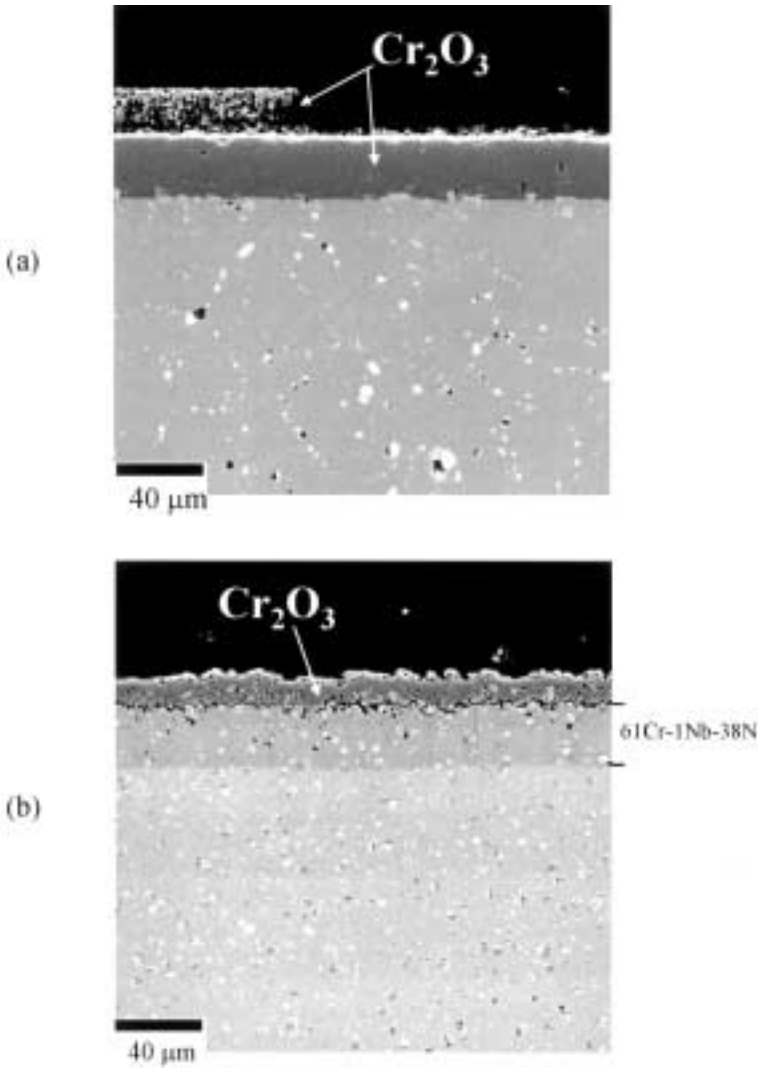

Fig. 5. Cross-section SEM (secondary mode) micrographs of the Cr–2.5Nb exposed at 1100°C for 24 hr in humid air. (a) Lower-weight change sample from Fig. 2b; (b) higher-weight change sample from Fig. 2b. The light particles present in the matrix in both alloys were Cr_2Nb Laves-phase particles and Nb-rich oxide inclusions.

The CP and HP Cr–2.5Nb coupons exposed for 120 hr in humid air exhibited extensive nitride subscale formation, on the order of 250 to 300 μm. In contrast, the lower weight gains for the unalloyed Cr and Cr–1Nb samples exposed for 120 hr at 1100°C in humid air (Fig. 3) were associated with much reduced subscale nitridation, on the order of 75 to100 μm for Cr–1Nb and 25–50 μm for unalloyed Cr. The microstructures were qualitatively similar to that shown in Fig. 5b.

Cr_2Nb Phase: Cr–31Nb

Some spallation was observed for Cr–31Nb exposed for 24 hr at 1100°C in either dry or humid air. In both cases, the outer-scale regions were quite similar and consisted of a seemingly dense, continuous Cr_2O_3 layer approximately 10 μm thick, with an additional zone of disconnected Cr_2O_3 particles at the scale–gas interface (Fig. 6) similar to that observed for Cr–2.5Nb (Fig. 5a). For the dry air-exposure sample, a multilayered region approximately 40 μm deep was evident underneath the Cr_2O_3 scale. It consisted of an approximately 10-μm thick region of Cr–Nb oxide overlying a partially oxidized 10-μm thick Cr–Nb nitride (oxygen ranging from 0.5 to 8 at.% and nitrogen ranging from 15 to 33 at.%), itself overlying a 10- to 20-μm thick, nitrogen-containing region of average composition 60Cr–28Nb–12N (Fig. 6a).

In contrast, Cr–31Nb exposed in humid air formed a 40–50 μm thick region of mixed Cr–Nb oxides overlying a 100–150 μm deep region of nitride subscale (Fig. 6b). The nitride subscale formed in humid air consisted primarily of a 100-μm deep region, ranging in composition from 43Cr–22Nb–35N at the outermost edge to 53Cr–24Nb–23N at the innermost edge. It likely was composed of a very fine mixture of at least two phases (not visible in Fig. 6b). Extending beyond this 35–23 at.% nitrogen subscale region was an additional zone of decreasing nitrogen content, from 61Cr–29Nb–10N downward in nitrogen content with increasing depth into the alloy, extending approximately an additional 25–50 μm. At the interface between the Cr–Nb oxide region and the nitride subscale was a transition oxynitride-gradient region, similar to that observed in dry air, which likely formed by subsequent oxidation of the nitride subscale.

Two-Phase Cr(Nb)+Cr_2Nb Eutectic: Cr–18.5Nb

As with Cr–31Nb, comparatively little nitridation was observed for Cr–18.5Nb exposed for 24 hr at 1100°C in dry air as compared with a humid air exposure (Fig. 7a and b). The scale formed in dry air spalled completely during cooling (Fig. 7a). A small region of oxynitride was retained at the metal–scale interface, with average composition of 34Cr–36Nb–5O–25N.

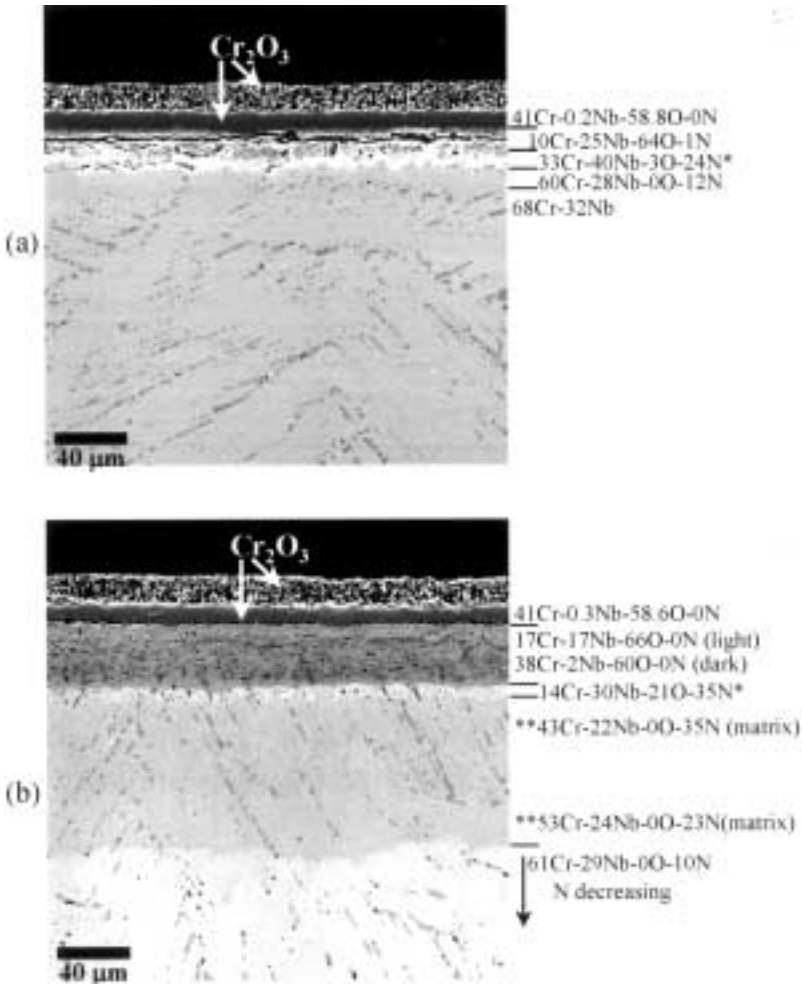

Fig. 6. Cross-section SEM (secondary mode) micrographs of the Cr–31Nb samples from Fig. 2. (a) Filtered compressed dry air, 1100°C, 24 hr; (b) humid air, 1100°C, 24 hr. The minor (dark) second phase present in the Cr_2Nb Laves phase matrix is the Cr(Nb) phase. *, Gradient in oxygen and nitrogen level detected within this zone, with decreasing oxygen and increasing nitrogen with greater depth, **, Average composition, the nitrided-Laves phase consisted of a very fine mixture of at least two phases.

Underneath this, a nitrogen gradient was detected in the Laves-phase matrix, with compositions in the range of (50–60)Cr–(30–35)Nb–(4–13)N decreasing in N content toward the bulk of the alloy. The Cr(Nb) phase in this region was metallic and contained no nitrogen (as determined by EPMA

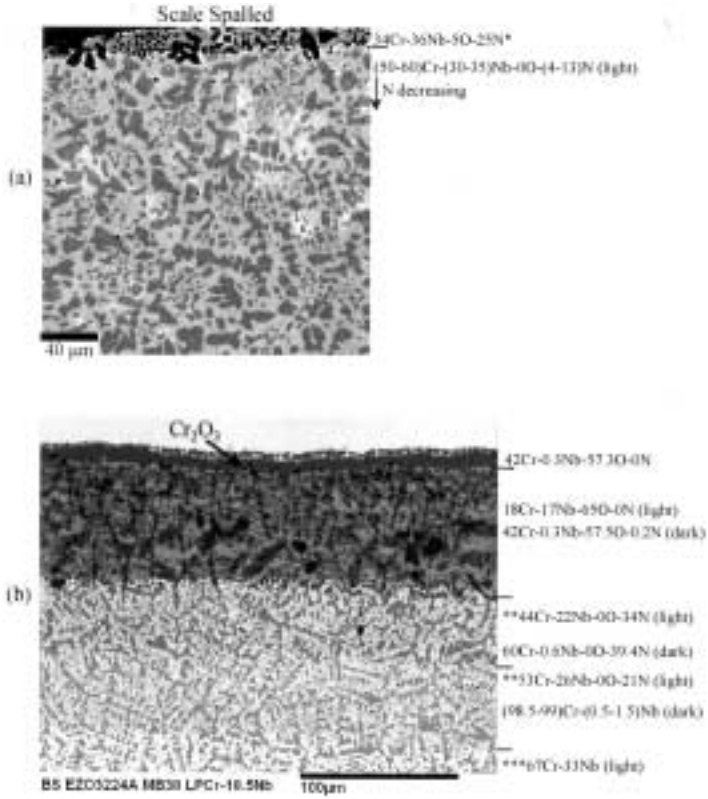

Fig. 7. Cross-section SEM (secondary mode) micrographs of the Cr–18.5Nb samples from Fig. 2. The light-phase matrix in the alloy is the Cr_2Nb Laves phase. The dark second phase is the Cr(Nb) phase. (a) Filtered compressed dry air, 1100°C, 24 hr; (b) humid air, 1100°C, 24 hr. *, Data obtained from a similarly exposed sample; **, average composition; the nitrided-Laves phase consisted of a very fine mixture of at least two phases; ***, nominal Cr : Nb ratio; some data points in this region indicated the presence of nitrogen (<20 at.%), decreasing with depth.

analysis). The depth of the nitrogen-gradient region in the Laves phase showed some variation from point to point and sample to sample, and was, therefore, difficult to determine. A qualitative estimate would be less than 25–50 μm beyond the metal–scale interface. (Note that the dry air, 1100°C, 24-hr exposed HP Cr–18.5Nb coupon shown in Fig. 4, which exhibited an increase in oxidation rate at about 15 hr of exposure, showed evidence of more extensive nitridation, on the order of 100 μm total nitrogen penetration).

The scale formed in humid air was relatively adherent. It consisted of a continuous layer of Cr_2O_3, ranging from 15 to 30 μm thick (including outer, friable zone) overlying a region of mixed Cr + Nb oxides (primarily $CrNbO_4$ and Cr_2O_3 based on XRD analysis) on the order of 100 μm thick (Fig. 7b). As with Cr–31Nb exposed in humid air (Fig. 6b), an extensive nitride subscale was evident (Fig. 7b). The nitridation mimicked the underlying alloy microstructure with the Cr(Nb) and Cr_2Nb phases nitriding independently. This form of attack, in which oxidation (or nitridation, etc.) follows the underlying alloy microstructure, has been termed *in situ* or *in place* internal oxidation because the underlying alloy microstructure is consumed in place.[16–18] Consistent with this process, the stoichiometry of the nitrided-Laves phase retained the 2Cr : 1Nb ratio of metallic Cr_2Nb Laves phase (Fig. 7b).[18] XRD of a sample, in which the external scale was removed by grinding, as well as SEM analysis, strongly suggested that the *in situ* nitrided-Laves phases consisted of a fine mixture of at least two phases, CrNbN and Cr_2N, which is consistent with the average composition in this region and the apparent nonexistence of a nitride of stoichiometry "Cr_2NbN" (phase equilibria in the Cr–Nb–N system is not well defined).

The nitride subscale consisted of three layers: an outer 40 to 50-μm region in which both Cr(Nb) and Cr_2Nb phases were nitrided (60Cr–0.6Nb–39.4N and 44°Cr–22Nb–34N, respectively), a second layer an additional 50-μm deep in which the Cr(Nb) phase was metallic (not nitrided), while the Cr_2Nb phase was preferentially nitrided (53Cr–26Nb–21N), and a third zone of decreasing N content in the Cr_2Nb phase (<10 at.% N) and metallic Cr(Nb) phase. Again, it was difficult to estimate the depth of the nitrogen-gradient region in the Cr_2Nb Laves phase. A qualitative estimate would be less than 10–80 μm beyond the interface with the Cr(Nb) + preferentially nitrided Cr_2Nb (53Cr–26Nb–21N) region.

Nitridation at 1100°C in N_2–$4H_2$

In order to further study the extensive subscale nitridation of the Cr(Nb) and Cr_2Nb phases that was observed after exposure in air, Cr–2.5Nb, Cr–18.5Nb, and Cr–31Nb samples were exposed in N_2–$4H_2$ at 1100°C for 24 hr (all CP alloys). Examination of cross sections showed structures similar to the nitride-subscale regions formed in air. (Note that external oxide-scale formation was not evident by SEM analysis in the N_2–$4H_2$-exposed samples. An obvious discrete external nitride scale was also not observed.) However, the depth of nitridation was significantly greater in N_2–$4H_2$ than in either dry or humid air (Fig. 8). This important result indicates that the extent of subscale nitridation in air was controlled by nitrogen penetration through the oxide scale rather than by nitrogen diffusion in the alloy.

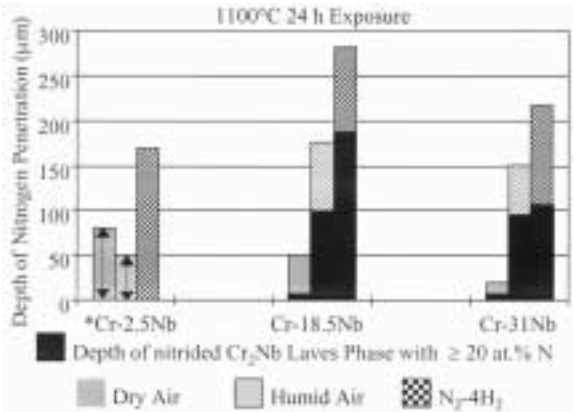

Fig. 8. Nitrogen-penetration depths for 24-hr exposure at 1100°C in filtered compressed dry air, humid laboratory air, and N_2–$4H_2$. *, Arrows show sample-to-sample range in nitridation depth for Cr–2.5Nb. Data shown are for CP alloys.

The tendency of the Cr_2Nb Laves phase to exhibit a two-layer nitrided zone of different average nitrogen contents (~35 at.% N content, ~20 at.% N content) followed by an additional region with a gradient in nitrogen content downward from approximately 10 at.% nitrogen (see Figs. 6 and 7) makes it difficult to meaningfully compare nitridation depth with that of the Cr(Nb) phase, which formed a single nitride layer of 38 to 40 at.% N (Cr_2N) with a sharp transition to Cr(Nb) metal. The depth of the nitrided region in the single-phase Cr_2Nb alloy Cr–31Nb, containing at least 20 at.% nitrogen, was less than the total nitridation depth in the single-phase Cr(Nb) alloy Cr–2.5Nb after 24 hr in N_2–$4H_2$ at 1100°C (consistent with specific weight-change measurements). However, the total depth of nitrogen penetration in the single-phase Cr_2Nb alloy Cr–31Nb (which includes the nitrogen-gradient zone from ~10 to 0 at.% nitrogen) was similar to/somewhat greater than the total depth of nitrogen penetration to the Cr(Nb) phase alloy Cr–2.5Nb in N_2–$4H_2$. Overall, these data strongly suggest that the extensive preferential nitridation of the Cr_2Nb Laves phase in the two-phase Cr(Nb) + Cr_2Nb eutectic alloy Cr–18.5Nb (Fig. 7) was not the result of higher nitrogen diffusivity in the Laves phase relative to the Cr(Nb) solid-solution phase. It is interesting to note that the >20 at.% nitrogen-zone depth and total depth of nitridation in Cr–18.5Nb was moderately greater than that in either Cr–2.5Nb, single-phase Cr(Nb), or Cr–31Nb, single-phase Cr_2Nb, which is suggestive of a degree of preferential nitrogen transport down the interface between the two phases.

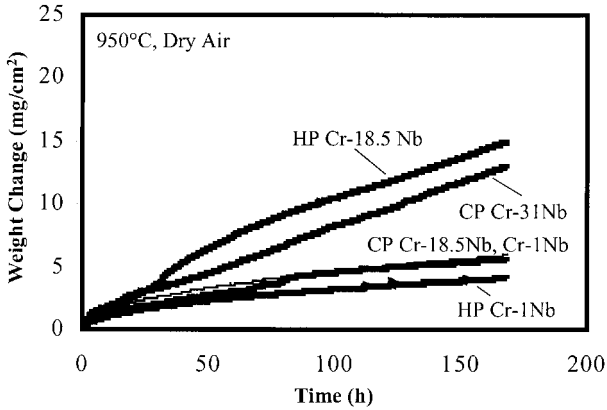

Fig. 9. TGA data at 950°C in filtered compressed dry air for CP Cr–31Nb, CP and HP Cr–18.5Nb, and CP and HPCr–1Nb.

Finally, 24-hr exposures at 1100°C in N_2–$4H_2$ were also conducted for unalloyed Cr and Cr–1Nb, which showed nitridation depths of 205 and 185 μm, respectively. This compares with 170-μm depth of nitridation for Cr–2.5Nb. Therefore, the presence of Nb in solution in Cr did not increase nitrogen diffusivity in the alloy.

Oxidation Behavior at 950°C

Figure 9 shows TGA data for CP and HP Cr–1Nb, CP and HP Cr–18.5Nb, and CP Cr–31Nb oxidized for 1 week at 950°C in dry air. Near-parabolic oxidation kinetics were observed for both CP and HP Cr–1Nb, with the differences in oxidation rate between the two samples within the range of scatter observed for Cr(Nb) alloys under the conditions studied. In contrast, a significant effect of oxygen- and sulfur-impurity level was observed for Cr–18.5Nb, with HP Cr–18.5Nb showing much more rapid (and linear) oxidation kinetics as compared to CP Cr–18.5Nb, which exhibited relatively slow, near-parabolic behavior. The CP Cr–31Nb alloy exhibited rapid linear-oxidation kinetics similar to that of HP Cr–18.5Nb. (An HP Cr–31Nb sample was not oxidized under these conditions.)

The major difference between CP and HP Cr–18.5Nb was the level of oxygen and sulfur impurities, with the CP alloy containing 4711 wppm oxygen and 220 wppm sulfur, while the HP alloy contained less than 29 wppm oxygen and <10 wppm sulfur (Table I). To further investigate this effect, a series of HP alloys were cast and intentionally doped with oxygen (4947 wppm oxygen and 30 wppm sulfur) or sulfur (172 wppm oxygen and 280 wppm sulfur) by adding Cr_2O_3 or Cr_2S_3 to the arc-melt charge. Unlike

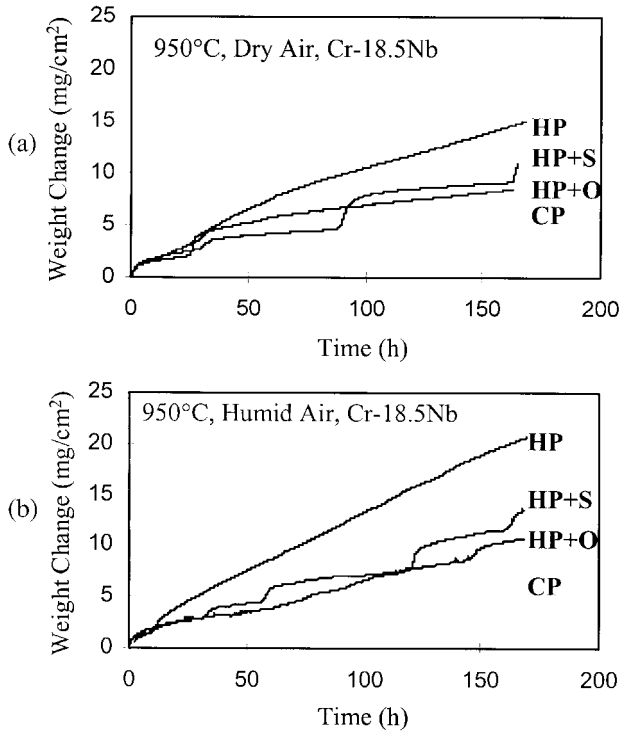

Fig. 10. TGA data at 950°C for CP Cr–18.5Nb, HP Cr–18.5Nb, and HP Cr–18.5Nb with additions of oxygen (O) or sulfur (S). (a) Filtered compressed dry air; (b) humid air.

oxidation behavior at 1100°C, little difference between dry- and humid-air exposure was observed at 950°C, although oxidation of HP Cr–18.5Nb was moderately more rapid in humid air (Fig. 10). Rather, impurity effects dominated behavior with high levels of both oxygen and sulfur (CP alloy) leading to lower oxidation kinetics. The TGA curves for oxygen or sulfur-doped Cr–18.5Nb show reaction rates intermediate to that of HP and CP Cr–18.5Nb (Fig. 10), with discontinuities in the curves (particularly sulfur doped) typical of scale-cracking events.[19] For comparative purposes, un-alloyed Cr with three different levels of impurities (CP, HP, and UHP, see Table I) was oxidized at 950°C, with no major effect of impurity level detected (Fig. 11).

Cross-section SEM analysis of the Cr–18.5Nb samples exposed for 1 week at 950°C revealed that the CP alloy exhibited little subscale nitridation (Fig. 12a), while the HP alloy exhibited an extensive nitride subscale (Fig.

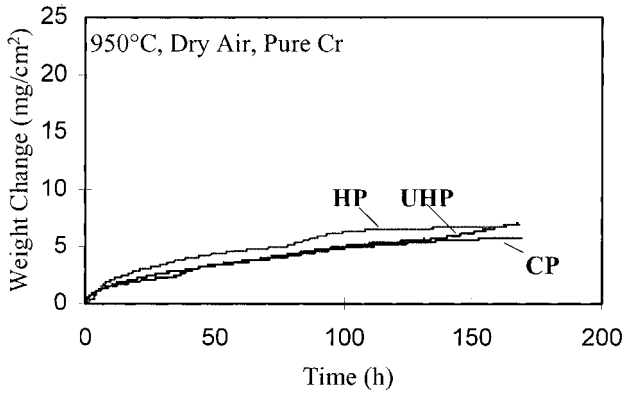

Fig. 11. TGA data at 950°C in filtered compressed dry air for CP, HP, and UHP Cr.

12b). Subscale nitridation also occurred in both the HP + oxygen (Fig. 12c) and HP + sulfur Cr–18.5Nb (Fig. 12d), but not to the same extent as was observed for HP Cr–18.5Nb (Fig. 12b). Interestingly, the Cr(Nb) + Cr_2Nb alloy microstructures in the CP Cr–18.5Nb and oxygen-doped Cr–18.5Nb were much coarser than those of the HP and HP + S Cr–18.5Nb (compare Figs. 12a, c with b, d). The reasons for this are not known, but are suspected to be related to the presence of oxide inclusions in the CP material, which may have affected nucleation/growth of the eutectic structure during solidification and cooling of the alloy after casting. In a similar manner to what was observed at 1100°C (Fig. 7), the nitridation of the Cr–18.5Nb at 950°C mimicked the underlying alloy microstructure with the Cr(Nb) and Cr_2Nb phases reacting independently. Again, the Cr_2Nb Laves phase was nitrided to a greater depth than the Cr(Nb) phase [in Fig. 12, region 1 marks where both the Cr(Nb) and Cr_2Nb phases were nitrided and region 2 marks where the Cr_2Nb phase alone was nitrided]. The *in place*, internal-nitridation phenomenon for these alloys is discussed in greater detail in Refs. 11, 13, and 14.

The scales formed on Cr–18.5Nb after 1 week at 950°C at all levels of impurities (Fig. 12) consisted of alternating layers of Cr_2O_3 and Nb–Cr rich oxides (primarily $CrNbO_4$). The Cr_2O_3 bands in the CP and HP + oxygen samples were much coarser than in the HP sample and, perhaps, moderately coarser than in the HP + S sample, which qualitatively correlated with the coarseness of the underlying alloy microstructure. The banding also qualitatively correlated with the discontinuities present in the TGA curves (Fig. 10), with few discontinuities in the CP and HP + oxygen curves consistent with the coarser banding observed for these alloys; this suggests interrupted

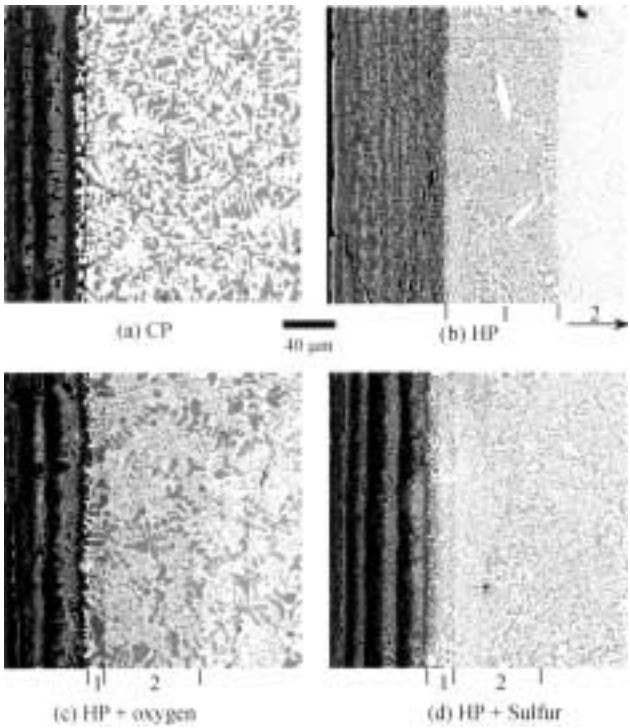

Fig. 12. Cross-section SEM (secondary mode) micrographs of the Cr–18.5Nb samples from Fig. 10b after 168 hr at 950°C in humid air. (a) CP; (b) HP; (c) HP + oxygen; (d) HP + sulfur. The light matrix phase is the Cr_2Nb Laves phase. The dark second phase is the Cr(Nb) phase. Region 1 is where both Cr_2Nb and Cr(Nb) phases are nitrided. Region 2 is where the Cr_2Nb Laves phase is nitrided, Cr(Nb) is metallic. The dark banded oxide in the scale is Cr_2O_3. The light-banded oxide in the scale is mixed Cr + Nb oxide (primarily $CrNbO_4$).

periods of moderately protective Cr_2O_3 scale growth. The greater number of discontinuities in the HP + S sample (and a somewhat finer banding) suggest shorter periods of protection by Cr_2O_3. The TGA curve for the HP sample showed rapid linear-oxidation kinetics, which is consistent with very short or negligible times during which oxidation was controlled by growth of protective Cr_2O_3.

DISCUSSION

Exposure in humid air relative to dry air significantly increased the nitrogen permeability of the scale formed at 1100°C on both Cr–18.5Nb, the Cr(Nb)–Cr_2Nb eutectic composition (Cr_2Nb continuous), and Cr–31Nb,

single-phase Cr_2Nb (Fig. 8). Little effect of the level of oxygen or sulfur impurities was noted at 1100°C. In contrast, at 950°C, little effect of humid- vs. dry-air was noted for Cr–18.5 Nb. However, the level of oxygen and sulfur impurities had a major effect, with significantly increased nitrogen penetration for HP Cr–18.5Nb compared to CP Cr–18.5Nb. (Figs. 9 and 10). (Extensive humid vs. dry air and CP vs. HP alloy exposures were not conducted for Cr–31Nb because of complications associated with the extreme brittleness of this alloy, which resulted in cracked and irregular-shaped test coupons; this made normalization of oxidation kinetics difficult.) Although there was some variability from sample to sample, there was little difference in subscale nitrogen penetration with dry air/humid air and/or oxygen/sulfur impurity level for the single-phase Cr(Nb) alloys Cr–2.5Nb and Cr–1Nb and unalloyed Cr, respectively, at 1100 or 950°C. (Differences in subscale nitrogen penetration between unalloyed Cr, Cr–1Nb, and Cr–2.5Nb did exist and are discussed at the end of this section.)

Zheng and Young[20,21] and Young and Watson[22] have reported reduced, not increased, nitrogen permeation in Cr_2O_3 scales formed on unalloyed Cr at 900°C in 56.5 H_2–2.3 H_2O–41.2N_2 vol.% gas (compared to reactions in 62.2CO–2.2CO_2–35.6N_2; the oxygen and nitrogen activities in the gases were equivalent). These findings suggest that, in the present case, the water vapor present in humid laboratory air may not have directly increased nitrogen transport in the Cr_2O_3 scale formed on Cr–18.5Nb.

Zheng and Young[20,21] also reported reduced nitrogen permeation in Cr exposed at 900°C in CO–CO_2–SO_2–N_2 gases (e.g., 62.2CO–2.18CO_2–35.6N_2–0.01SO_2 vol.%) as compared to exposure in 62.2CO–2.2CO_2–35.6N_2 vol.%, in which subscale nitridation of Cr occurred. In this case, it was hypothesized that preferential adsorption of sulfur on oxide boundaries and internal interfaces blocked nitrogen uptake. Based on this, it is speculated that the sulfur impurities present in the CP Cr–18.5Nb segregated to the scale and reduced nitrogen permeability at 950°C. Such segregation is consistent with work by Fox *et al.*,[23] which showed that sulfur impurities present in unalloyed Cr segregate to the metal–oxide interface and oxide grain boundaries during oxidation at 950°C (reported impurity levels of 8900 wppm oxygen and 100 wppm sulfur). The level of sulfur in HP Cr–18.5Nb may have been sufficiently low (<10 wppm), that sulfur segregation to the scale at 950°C did not occur to an extent sufficient to significantly retard nitrogen adsorption and penetration under the conditions studied. At 1100°C, the additional thermal energy is thought to sufficiently increase outward sulfur segregation to the scale such that the lower level of bulk sulfur present in HP Cr–18.5Nb could then retard nitrogen adsorption and penetration, at least in dry air.

The behavior at 950°C of HP + oxygen and HP + sulfur Cr–18.5Nb partially supports the above speculation. The TGA data indicated intermediate oxidation rates to that of HP and CP Cr–18.5Nb (Fig. 10), and the cross-section SEM analysis (Fig. 12) showed subscale nitridation in both the HP + oxygen and HP + sulfur Cr–18.5Nb, but not to the same extent as was observed for HP Cr–18.5Nb. The presence of high levels of oxygen impurities in Cr–18.5Nb was observed to result in a coarser Cr_2Nb + Cr(Nb) microstructure, which qualitatively correlated with the thickness of the Cr_2O_3 layers present in the banded Cr_2O_3–$CrNbO_4$ scales formed on these alloys at 950°C. It is suspected that the coarse microstructure in the CP and HP + O samples contributed to the formation of the coarser Cr_2O_3 bands, which, if dense, can act as a more effective barrier to nitrogen and better retard subscale nitridation. The reduced nitrogen permeability in CP Cr–18.5Nb at 950°C, therefore, appears to be the result of a complex, synergistic interaction between oxygen and sulfur impurities, rather than solely a sulfur effect.

A key question arising from the present results is whether the increased nitrogen permeability in Cr–18.5Nb at 1100°C in humid air was related to the increased subscale nitridation for Cr–18.5Nb observed at 950°C for lower levels of oxygen and sulfur impurities. It is important to note that study of the oxidation behavior of Cr–31Ta, a single-phase Cr_2Ta Laves-phase alloy, indicated extensive nitridation at 1100°C, similar to that observed for Cr–31Nb at 1100°C in humid air (no effect of humid vs. dry air or CP vs. HP impurity levels was observed for alloys in the Cr(Ta)–Cr_2Ta system).[11,14] This result suggests that the absence of extensive subscale nitridation in dry air at 1100°C for Cr–18.5Nb and Cr–31Nb is the anomalous effect, *not* the extensive nitridation in humid air.

One possible explanation of the apparent anomaly related to dry vs. humid air is an *in situ* desulfurization of the scale formed at 1100°C on Cr–18.5Nb (and Cr–31Nb) by interaction between the water vapor present in the humid air and sulfur impurities segregated to the scale. Such *in situ* desulfurization was postulated by Quadakkers *et al.*[24] to occur for oxidation of Cr-base alloys at 950°C in an Ar–4%H_2–2%H_2O environment. The removal of sulfur from the scale formed on Cr–18.5Nb at 1100°C in humid air would eliminate the suspected retarding effect of sulfur on nitrogen adsorption (again, Zheng and Young[20,21] demonstrated reduced subscale nitridation for Cr in the presence of small amounts of SO_2), resulting in greater nitrogen penetration through the scale. At 950°C, for Cr–18.5Nb under the conditions studied, there may be insufficient thermal energy available for scale desulfurization to occur.

It was shown that the nitrogen permeability of the scales formed on Cr–18.5Nb was affected by humidity and oxygen/sulfur-impurity levels, but

that the scale on Cr–2.5Nb was not very sensitive to these conditions. The reasons for this are not clear. There appears to be a significant difference in the local microstructure or chemistry (and subsequent nitrogen-transport paths) of the Cr_2O_3-base scales formed on Cr_2Nb-matrix alloys compared to Cr(Nb) solid-solution alloys (and unalloyed Cr). The addition of Nb in solution to Cr was found to increase the nitrogen permeability of the Cr_2O_3 scale that was formed, with unalloyed Cr, Cr–1Nb, and Cr–2.5Nb showing nitridation depths on the order of 25 to 50 μm, 75 to 100 μm, and 250 to 300 μm, respectively, after 120-hr exposures at 1100°C. This effect may have contributed to the sample-to-sample variation observed in the oxidation behavior of the Cr(Nb) alloys, with minor local differences in Nb content in a given sample and from sample-to-sample affecting the degree to which nitrogen permeated the scale.

Finally, it is interesting to note that anomalous oxidation behavior in dry and humid air has been observed in at least one other developmental intermetallic-alloy system in which both oxidation and nitridation can occur. A γ-TiAl base alloy of composition Ti–52Al–5Cr at.% showed protective oxidation kinetics and alumina-scale formation at 1000°C in dry air, but suffered from rapid oxidation and extensive nodule formation on open exposure to humid laboratory air.[25] The nodular structure was banded and exhibited extensive nitridation at the alloy–nodule interface. Similar behavior was not observed at 800°C, with relatively high rates of oxidation observed in both dry air and humid air. The detrimental effect of humid air at 1000°C was originally speculated to be the result of stabilization of the β-Ti phase in the alloy by ingress of hydrogen from the water vapor present in humid laboratory air. However, in light of the present results, this effect may have been related to a similar impurity effect to that observed/postulated here. Anomalous subscale nitridation was also recently reported in Fe_3Al alloys, the cause of which was not isolated.[26] It is possible that such behavior may be common, especially in developmental intermetallic alloys, which are often borderline with regards to protective scale formation and often contain base elements, which are very stable thermodynamically with several oxidants. It also suggests the possibility of controlled doping of the impurity levels to improve oxidation resistance, although intentional doping of alloys with sulfur clearly raises issues regarding scale adhesion under cyclic conditions [e.g., Ref. 27].

SUMMARY AND CONCLUSIONS

1. The Cr(Nb)–Cr_2Nb eutectic alloy Cr–18.5Nb and the single-phase Laves alloy Cr–31Nb exhibited anomalously low oxidation rates at 1100°C in dry air as compared with humid air. The low rates were associated with

greatly reduced subscale nitridation in dry air. This effect was speculated to result from *in situ* desulfurization of the scale during exposure in humid air, which, by removing sulfur, freed sites for nitrogen adsorption.

2. The Cr(Nb)–Cr_2Nb eutectic alloy Cr–18.5Nb exhibited an anomalously low oxidation rate at 950°C in dry or humid air when a high level of oxygen and sulfur impurities were present in the alloy. The low rate was associated with greatly reduced subscale nitridation. This effect was thought to result from a synergistic beneficial combination of a coarse two-phase microstructure resulting from the presence of oxygen impurities/oxide inclusions, which led to coarser bands of Cr_2O_3 in the banded Cr_2O_3/$CrNbO_4$ scales that formed, and blocking of nitrogen adsorption sites by segregation of sulfur from the alloy to the scale.

3. Little effect of oxygen- and sulfur-impurity level or dry vs. humid air exposure was observed for the oxidation behavior of unalloyed Cr and the Cr(Nb) solid-solution alloy Cr–2.5Nb at 950 or 1100°C. The addition of Nb in solution to Cr was observed to increase the nitrogen permeability of the scale, resulting in increased subscale nitridation.

ACKNOWLEDGMENTS

The authors thank J. A. Haynes, B. A. Pint, and I. G. Wright for reviewing this manuscript. This research was sponsored by the U.S. Department of Energy, Fossil Energy Advanced Research Materials (ARM) Program. Oak Ridge National Laboratory is managed by UT-Battelle, LLC for the U.S. Department of Energy under contract DE-AC05-00OR22725.

REFERENCES

1. M. Mazdiyasni and D. B. Miracle, in *Intermetallic Matrix Composites*, D. L. Anton, P. L. Martin, D. B. Miracle, and R. McMeeking, eds. (MRS, Pittsburgh, PA, 1990), pp. 155–162.
2. M. Takeyama and C. T. Liu, *Mater. Sci. Eng.* **A132**, 61 (1991).
3. L. W. Hobbs, C. Zhou, and J. C. Duncan, U.S. Patent 5,368,813 (1994).
4. B. P. Bewlay, J. A. Sutliff, M. R. Jackson, and H. A. Lipsitt, *Acta Mater.* **42**, 2869 (1994).
5. C. T. Liu, P. F. Tortorelli, J. A. Horton, and C. A. Carmichael, *Mater. Sci. Eng. A* **214**, 23 (1996).
6. K. S. Kumar and C. T. Liu, *Acta Mater* **45**, 3671 (1997).
7. N. Aoyama and S. Hanada, *Mater. Trans. JIM* **38**, 155 (1997).
8. M. Yoshida and T. Takasugi, *Mater. Sci. Eng. A* **224**, 77 (1997).
9. K. S. Ravichandran, D. B. Miracle, and M. G. Mendiratta, *Metall. Mater. Trans. A* **27**, 2583 (1996).
10. M. P. Brady, J. H. Zhu, C. T. Liu, P. F. Tortorelli, L. R. Walker, C. G. McKamey, J. L. Wright, C. A. Carmichael, D. J. Larson, M. K. Miller, and W. D. Porter, *Mater. High Temp.* **16**, 189 (1999).
11. M. P. Brady, J. H. Zhu, C. T. Liu, P. F. Tortorelli, and L. R. Walkerm, *Intermetallics* **8**, 1111 (2000).

12. W. D. Klopp, NASA Tech. Memorandum, NASA TM X-1867 (Sept., 1969).
13. M. P. Brady, P. F. Tortorelli, and L. R. Walker, *Mater. High Temp.* **17**, 235 (2000).
14. M. P. Brady, P. F. Tortorelli, I. M. Anderson, and L. R. Walker, Oxid. Met., submitted.
15. D. J. Thoma and J. H. Perepezko, *Mater. Sci. Eng.* **A156**, 97 (1992).
16. F. Gesmundo, Y. Niu, and F. Viani, *Oxid. Met.* **43**, 379 (1995).
17. F. Gesmundo and B. Gleeson, *Oxid. Met.* **44**, 211 (1995).
18. M. P. Brady, D. T. Hoelzer, E. A. Payzant, P. F. Tortorelli, J. A. Horton, I. M. Anderson, L. R. Walker, and S. K. Baham, *J. Mater. Res.* **16**, 2784 (2001).
19. P. Kofstad, *High Temperature Corrosion* (Elsevier Appl. Sci., Amsterdam, 1988).
20. X. G. Zheng and D. J. Young, *Corros. Sci.* **36**, 1999 (1994).
21. X. G. Zheng and D. J. Young, *Oxid. Met.* **42**, 163 (1994).
22. D. J. Young and S. Watson, *Oxid. Met.* **44**, 239 (1995).
23. P. Fox, D. G. Lees, and G. W. Lorimer, *Oxid. Met.* **36**, 491 (1991).
24. W. J. Quadakkers, J. F. Norton, S. Canetoli, K. Schuster, and A. Gil, in *Microscopy of Oxidation 3*, S. B. Newcomb and J. A. Little, eds. (The Institute of Metals, London, 1997), pp. 609–619.
25. M. P. Brady, J. L. Smialek, D. L. Humphrey, and J. W. Smith, *Acta Mater.* **45**, 2371 (1997).
26. B. A. Pint, J. R. Regina, K. Pruessner, L. D. Chitwood, K. B. Alexander, and P. F. Tortorelli, *Intermetallics* **9/8**, 735.
27. J. L. Smialek, *JOM* **52**, 22 (2000).